Journal of Computational Physics 299 (2015) 82–91

Contents lists available at ScienceDirect

Journal of Computational Physics

www.elsevier.com/locate/jcp

First and second order operator splitting methods for the phase field crystal equation

Hyun Geun Lee [a], Jaemin Shin [a], June-Yub Lee [b,*]

[a] Institute of Mathematical Sciences, Ewha Womans University, Seoul 120-750, Republic of Korea
[b] Department of Mathematics, Ewha Womans University, Seoul 120-750, Republic of Korea

ARTICLE INFO

Article history:
Received 16 October 2014
Received in revised form 8 May 2015
Accepted 30 June 2015
Available online 3 July 2015

Keywords:
Phase field crystal
Operator splitting method
First and second order convergences
Fourier spectral method

ABSTRACT

In this paper, we present operator splitting methods for solving the phase field crystal equation which is a model for the microstructural evolution of two-phase systems on atomic length and diffusive time scales. A core idea of the methods is to decompose the original equation into linear and nonlinear subequations, in which the linear subequation has a closed-form solution in the Fourier space. We apply a nonlinear Newton-type iterative method to solve the nonlinear subequation at the implicit time level and thus a considerably large time step can be used. By combining these subequations, we achieve the first- and second-order accuracy in time. We present numerical experiments to show the accuracy and efficiency of the proposed methods.

1. Introduction

Material properties at the meso- and macro-scales are to a large extent controlled by complex microstructures exhibiting topological defects, such as vacancies, grain boundaries, and dislocations. An understanding of formation and evolution of these defects is of great interest, and defects pose significant challenges to modeling and simulation because of the complexity they introduce. Recently, a new model called the phase field crystal (PFC) model for simulating defects has been proposed by Elder et al. [1,2]. This model describes the microstructure of two-phase systems on atomic length scales but on diffusive time scales, leading to significant computational savings compared to molecular dynamics simulations which are limited by atomic length scales and femtosecond time scales. In the PFC model, a phase-field formulation is introduced that accounts for the periodic structure of a crystal lattice through a free energy functional of Swift–Hohenberg type [3]

$$\mathcal{E}(\phi) := \int_{\Omega} \left(\frac{1}{4}\phi^4 + \frac{1-\epsilon}{2}\phi^2 - |\nabla\phi|^2 + \frac{1}{2}(\Delta\phi)^2 \right) d\mathbf{x}, \tag{1}$$

where $\phi : \Omega \subset \mathbb{R}^d \to \mathbb{R}$ $(d = 1, 2, 3)$ is the density field, ϵ is a positive constant with physical significance, and ∇ and Δ are the gradient and Laplacian operators, respectively. The PFC equation is derived from the energy functional $\mathcal{E}(\phi)$ under the constraint of mass conservation:

$$\frac{\partial\phi}{\partial t} = \nabla \cdot (M(\phi)\nabla\mu), \tag{2}$$

* Corresponding author.
E-mail address: jyllee@ewha.ac.kr (J.-Y. Lee).

http://dx.doi.org/10.1016/j.jcp.2015.06.038
0021-9991/

where $M(\phi) > 0$ is a mobility function and μ is the chemical potential defined as $\mu := \frac{\delta \mathcal{E}}{\delta \phi} = \phi^3 + (1-\epsilon)\phi + 2\Delta\phi + \Delta^2\phi$. $\frac{\delta \mathcal{E}}{\delta \phi}$ denotes the variational derivative of $\mathcal{E}$ with respect to ϕ. We assume that ϕ, $\Delta\phi$, and μ are periodic on Ω. Because (2) is of gradient type, it is easy to see that the energy functional $\mathcal{E}(\phi)$ is non-increasing in time. Taking $M(\phi) = 1$ for convenience, we obtain the PFC equation

$$\frac{\partial \phi}{\partial t} = \Delta(\phi^3 + (1-\epsilon)\phi + 2\Delta\phi + \Delta^2\phi). \tag{3}$$

The PFC equation is a sixth-order nonlinear partial differential equation. It is not easy to get an analytic solution in general, therefore, accurate and efficient numerical algorithms are essential in the computer simulations. Various computational algorithms [1,2,4–8] have been applied to solve the PFC equation numerically. In [1,2], Elder et al. use an explicit Euler method which is known to be unstable for time step Δt above a threshold proportional to $(\Delta x)^6$ where Δx is grid spacing. Thus, the explicit Euler method is computationally expensive to evolve large systems.

In [4], Cheng and Warren propose a method which improves the time step restriction considerably larger by splitting the linear terms into backward and forward pieces while treating the nonlinear term explicitly. In [5], Backofen et al. present a semi-implicit finite element method which is a backward Euler method, whereas the nonlinear term ϕ^3 in the chemical potential μ is linearized via $(\phi^{n+1})^3 \approx 3(\phi^n)^2\phi^{n+1} - 2(\phi^n)^3$. In [6], Hu et al. present first-order one-step and second-order two-step methods where a considerably large time step can be used by computing the nonlinear term at an implicit time level. However, an effective time step becomes smaller than the specified time step, as the authors observed for larger time steps.

We here present accurate and efficient operator splitting methods for solving the PFC equation that are first- and second-order time accurate. Operator splitting schemes have been and continue to be used for many types of evolution equations [9–12]. It is easy to construct a first-order solution $A(t^{n+1})$ of time evolution equation

$$\frac{\partial A}{\partial t} = f_1(A) + f_2(A)$$

by computing

$$A(t^n + \Delta t) \cong \left(\mathcal{S}_1^{\Delta t} \circ \mathcal{S}_2^{\Delta t}\right) A(t^n)$$

where $\mathcal{S}_1^{\Delta t}$ and $\mathcal{S}_2^{\Delta t}$ are the evolution operators for $\frac{\partial A}{\partial t} = f_1(A)$ and $\frac{\partial A}{\partial t} = f_2(A)$, respectively. Then a second-order scheme can be derived simply by symmetrizing the first-order scheme [10]:

$$A(t^n + \Delta t) \cong \left(\mathcal{S}_1^{\Delta t/2} \circ \mathcal{S}_2^{\Delta t} \circ \mathcal{S}_1^{\Delta t/2}\right) A(t^n).$$

A core idea of the proposed methods is to decompose the PFC equation into linear and nonlinear subequations, in which the linear subequation has a closed-form solution in the Fourier space. We apply a nonlinear Newton-type iterative method to solve the nonlinear subequation at the implicit time level and thus a considerably large time step can be used. In particular, we combine a half-time linear solver and a second-order nonlinear solver followed by a final half-time linear solver for a second-order method.

This paper is organized as follows. In Section 2, we propose new operator splitting methods for the PFC equation. Numerical experiments showing the accuracy and efficiency of the proposed methods are presented in Section 3. Finally, conclusions are drawn in Section 4.

2. Operator splitting methods for the phase field crystal equation

We consider the PFC equation (3) in two-dimensional space $\Omega = [0, L_1] \times [0, L_2]$. Let N_1 and N_2 be positive integers, $h_1 = L_1/N_1$ and $h_2 = L_2/N_2$ be uniform grid sizes, and Δt be the time step size. We denote $x_{l_1} = l_1 h_1$ and $y_{l_2} = l_2 h_2$ for $l_1 = 0, 1, \ldots, N_1 - 1$ and $l_2 = 0, 1, \ldots, N_2 - 1$. Let $\phi^n_{l_1 l_2}$ be the approximation of $\phi(x_{l_1}, y_{l_2}, t^n)$, where $t^n = n\Delta t$.

For simplicity of notation, we define the "*linear operator*" $\mathcal{L}^{\Delta t}$ as follows

$$\mathcal{L}^{\Delta t}(\phi(t^n)) := \phi(t^n + \Delta t), \tag{4}$$

where $\phi(t^n + \Delta t)$ is a solution of the linear differential equation

$$\frac{\partial \phi}{\partial t} = (1-\epsilon)\Delta\phi + 2\Delta^2\phi + \Delta^3\phi \tag{5}$$

with an initial condition $\phi(t^n)$. To solve the PFC equation with the periodic boundary condition, we employ the discrete Fourier transform $\widehat{\phi} = \mathcal{F}[\phi]$:

$$\widehat{\phi}_{k_1 k_2} = \sum_{l_1=0}^{N_1-1} \sum_{l_2=0}^{N_2-1} \phi_{l_1 l_2} e^{-i\left(x_{l_1}\xi_{k_1} + y_{l_2}\xi_{k_2}\right)}, \tag{6}$$

where $\xi_{k_1} = 2\pi k_1/L_1$ and $\xi_{k_2} = 2\pi k_2/L_2$ for $k_1 = 0, 1, \ldots, N_1 - 1$ and $k_2 = 0, 1, \ldots, N_2 - 1$. Then, we have an analytical formula for the evolution operator $\mathcal{L}^{\Delta t}$ in the discrete Fourier space

$$\mathcal{L}^{\Delta t}(\phi) = \mathcal{F}^{-1}\left[e^{A\Delta t}\mathcal{F}[\phi]\right], \tag{7}$$

where $A(k_1, k_2) = -(1-\epsilon)\left(\xi_{k_1}^2 + \xi_{k_2}^2\right) + 2\left(\xi_{k_1}^2 + \xi_{k_2}^2\right)^2 - \left(\xi_{k_1}^2 + \xi_{k_2}^2\right)^3$. We also define the "*nonlinear operator*" $\mathcal{N}^{\Delta t}$ as follows

$$\mathcal{N}^{\Delta t}(\phi(t^n)) := \phi(t^n + \Delta t), \tag{8}$$

where $\phi(t^n + \Delta t)$ is a solution of the nonlinear differential equation

$$\frac{\partial \phi}{\partial t} = \Delta \phi^3 \tag{9}$$

with an initial condition $\phi(t^n)$.

A first-order operator splitting method for the PFC equation can be represented as

$$\phi^{n+1} = \left(\mathcal{L}^{\Delta t} \circ \mathcal{N}_1{}^{\Delta t}\right)\phi^n, \tag{10}$$

where $\phi^n \cong \phi(t^n)$ and $\phi^{n+1} \cong \phi(t^n + \Delta t)$. To solve the evolution operator $\mathcal{N}_1{}^{\Delta t}$ with the first-order accuracy, we apply the backward Euler method to Eq. (9) and represent the resulting equation to the decoupling form by introducing the auxiliary variable ν as

$$\phi^{n+1} - \phi^n = \Delta t\, \Delta \nu^{n+1}, \tag{11}$$

$$\nu^{n+1} = \left(\phi^{n+1}\right)^3. \tag{12}$$

Because of the nonlinearity for ϕ^{n+1}, we linearize the nonlinear term at $\phi^{n,m}$ as

$$\left(\phi^{n+1}\right)^3 \approx \left(\phi^{n,m}\right)^3 + 3\left(\phi^{n,m}\right)^2\left(\phi^{n+1} - \phi^{n,m}\right) \tag{13}$$

for $m = 0, 1, \cdots$. We then get the nonlinear Newton-type iterative method as

$$\begin{bmatrix} I & -\Delta t\, \Delta \\ -3\left(\phi^{n,m}\right)^2 & I \end{bmatrix}\begin{bmatrix} \phi^{n,m+1} \\ \nu^{n,m+1} \end{bmatrix} = \begin{bmatrix} \phi^n \\ -2\left(\phi^{n,m}\right)^3 \end{bmatrix}, \tag{14}$$

where $\phi^{n,0} = \phi^n$. We can eliminate $\phi^{n,m+1}$ in (14) and obtain the following equation for $\nu^{n,m+1}$:

$$-3\Delta t\left(\phi^{n,m}\right)^2 \Delta \nu^{n,m+1} + \nu^{n,m+1} = 3\left(\phi^{n,m}\right)^2 \phi^n - 2\left(\phi^{n,m}\right)^3. \tag{15}$$

From the numerical solution $\nu^{n,m+1}$ of (15), we can obtain

$$\phi^{n,m+1} = \phi^n + \Delta t\, \Delta \nu^{n,m+1}. \tag{16}$$

And we set

$$\phi^{n+1} = \phi^{n,m+1} \tag{17}$$

if a relative l_2-norm of the consecutive error $\frac{\|\phi^{n,m+1} - \phi^{n,m}\|}{\|\phi^{n,m}\|}$ is less than *tol*.

In addition, a second-order operator splitting method for the PFC equation can be represented as

$$\phi^{n+1} = \left(\mathcal{L}^{\Delta t/2} \circ \mathcal{N}_2{}^{\Delta t} \circ \mathcal{L}^{\Delta t/2}\right)\phi^n. \tag{18}$$

To solve the evolution operator $\mathcal{N}_2{}^{\Delta t}$ with the second-order accuracy, we apply the Crank–Nicolson method to Eq. (9) and represent the resulting equation to the decoupling form by introducing the auxiliary variable ν as

$$\phi^{n+1} - \phi^n = \Delta t\, \Delta \nu^{n+\frac{1}{2}}, \tag{19}$$

$$\nu^{n+\frac{1}{2}} = \frac{\left(\phi^{n+1}\right)^3 + \left(\phi^n\right)^3}{2}. \tag{20}$$

Replacing $(\phi^{n+1})^3$ by $\left(\phi^{n,m}\right)^3 + 3\left(\phi^{n,m}\right)^2\left(\phi^{n+1} - \phi^{n,m}\right)$ as in (13) yields

$$\begin{bmatrix} I & -\Delta t\, \Delta \\ -\frac{3}{2}\left(\phi^{n,m}\right)^2 & I \end{bmatrix}\begin{bmatrix} \phi^{n,m+1} \\ \nu^{n,m+1} \end{bmatrix} = \begin{bmatrix} \phi^n \\ -\left(\phi^{n,m}\right)^3 + \frac{1}{2}\left(\phi^n\right)^3 \end{bmatrix} \tag{21}$$

and we also apply nonlinear iterations similar with (15)–(17).

3. Numerical experiments

In this section, we present examples to numerically demonstrate the accuracy and efficiency of the proposed operator splitting (OS) methods compared to the well-known energy stable (ES) methods by Hu et al. [6]. First two numerical examples show the convergence and effective time of two methods for a one-dimensional test problem. The third example shows time evolution of random perturbation in 2D. We then perform a simulation of the growth of a polycrystal in a supercooled liquid, which demonstrates the feasibility of the OS method in computing the evolution of large systems.

Here we briefly review the ES methods which will be used for the numerical comparisons. The first-order ES method can be summarized as follows:

$$\phi^{n+1} - \phi^n = \Delta t\, \Delta \mu^{n+1}, \tag{22}$$

$$\mu^{n+1} = (\phi^{n+1})^3 + (1-\epsilon)\phi^{n+1} + 2\Delta\phi^n + \Delta\kappa^{n+1}, \tag{23}$$

$$\kappa^{n+1} = \Delta\phi^{n+1}. \tag{24}$$

By applying the linearized nonlinear term (13) to (22)–(24), the following nonlinear iteration is considered,

$$\begin{bmatrix} I & -\Delta t\,\Delta & 0 \\ -3(\phi^{n,m})^2 - (1-\epsilon) & I & -\Delta \\ -\Delta & 0 & I \end{bmatrix} \begin{bmatrix} \phi^{n,m+1} \\ \mu^{n,m+1} \\ \kappa^{n,m+1} \end{bmatrix} = \begin{bmatrix} \phi^n \\ 2\Delta\phi^n - 2(\phi^{n,m})^3 \\ 0 \end{bmatrix}. \tag{25}$$

And the second-order ES method is

$$\phi^{n+1} - \phi^n = \Delta t\, \Delta \mu^{n+\frac{1}{2}}, \tag{26}$$

$$\mu^{n+\frac{1}{2}} = \frac{1}{4}(\phi^{n+1} + \phi^n)((\phi^{n+1})^2 + (\phi^n)^2) + \frac{1-\epsilon}{2}(\phi^{n+1} + \phi^n) + 3\Delta\phi^n - \Delta\phi^{n-1} + \Delta\kappa^{n+\frac{1}{2}}, \tag{27}$$

$$\kappa^{n+\frac{1}{2}} = \frac{1}{2}(\Delta\phi^{n+1} + \Delta\phi^n), \tag{28}$$

where $\phi^{-1} = \phi^0$. For (26)–(28), the following nonlinear iteration is considered,

$$\begin{bmatrix} I & -\Delta t\,\Delta & 0 \\ A_{21} & I & -\Delta \\ -\frac{1}{2}\Delta & 0 & I \end{bmatrix} \begin{bmatrix} \phi^{n,m+1} \\ \mu^{n,m+1} \\ \kappa^{n,m+1} \end{bmatrix} = \begin{bmatrix} \phi^n \\ b_2 \\ -\frac{1}{2}\Delta\phi^n \end{bmatrix}, \tag{29}$$

where $A_{21} = -\frac{1}{4}\left((\phi^{n,m})^2 + (\phi^n)^2\right) - \frac{1}{2}(1-\epsilon)$ and $b_2 = -\frac{1}{4}\left((\phi^{n,m})^2 + (\phi^n)^2\right)\phi^n - \frac{1}{2}(1-\epsilon)\phi^n + 3\Delta\phi^n - \Delta\phi^{n-1}$. One can also apply the nonlinear iterations (25) and (29) until a relative l_2-norm of the consecutive error of $\phi^{n,m+1}$ is less than *tol*. Then let ϕ^{n+1} to be $\phi^{n,m+1}$.

3.1. Numerical convergence with a smooth test function in 1D

We demonstrate the convergence of the OS methods with a numerical solution of the PFC equation with initial condition

$$\phi(x,0) = 0.07 - 0.02\cos\left(\frac{2\pi(x-12)}{32}\right) + 0.02\cos^2\left(\frac{\pi(x+10)}{32}\right) - 0.01\sin^2\left(\frac{4\pi x}{32}\right) \tag{30}$$

on a domain $\Omega = [0, 32]$. The numerical solution is evolved to time $T_f = 10$ with $\epsilon = 0.025$. The grid size is fixed to $h = 1/3$ which provides enough spatial accuracy (around 10 digits).

To estimate the convergence rate with respect to a time step Δt, simulations are performed by varying the time step $\Delta t = T_f/2^{12}, T_f/2^{11}, \ldots, T_f$. We use the iterative method to solve the discrete nonlinear system (11)–(12) and (19)–(20). The stopping criterion for the nonlinear m-iteration is that a relative l_2-norm of the consecutive error is less than a tolerance (10^{-10} in this example). The initial guess at each time level is taken from the solution at the previous time level.

The number of m-iterations averaged over the simulation time $0 < t = n\Delta t \le T_f$ is shown as a function of time step Δt in Fig. 1. In (14) and (21) for the OS methods, 2–3 iterations were involved in proceeding to the next time level. We believe that such a fast iterative convergence can be achieved since the successive iteration (14) is a Newton-type approximation of (11) and (12) for the first-order approximation. Likewise, (21) is a Newton-type approximation of (19) and (20) for the second-order.

Fig. 2 shows the relative l_2-errors at $T_f = 10$ for various time steps Δt. Here, the errors are computed by comparison with a quadruply over-resolved reference numerical solution. Both OS and ES methods provide the first- and second-order accuracy in time; however, the OS methods give two orders of magnitude higher accuracy where both OS and ES methods in the convergence region.

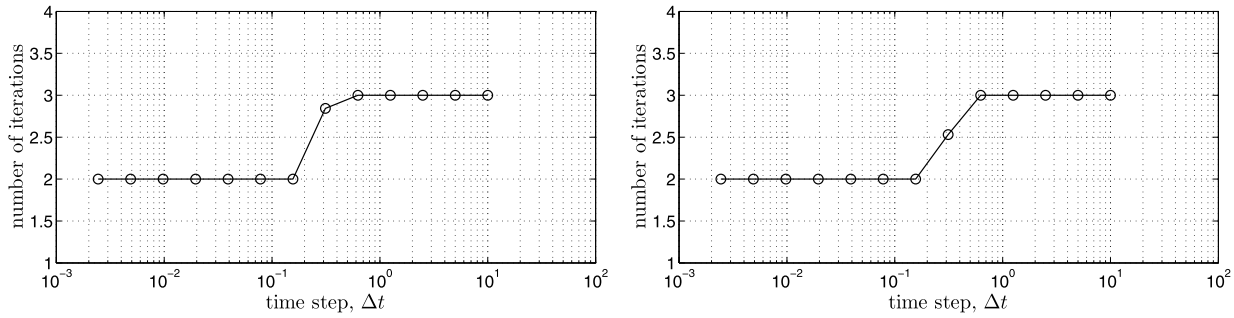

(a) First-order method (b) Second-order method

Fig. 1. Number of m-iterations averaged over the simulation time.

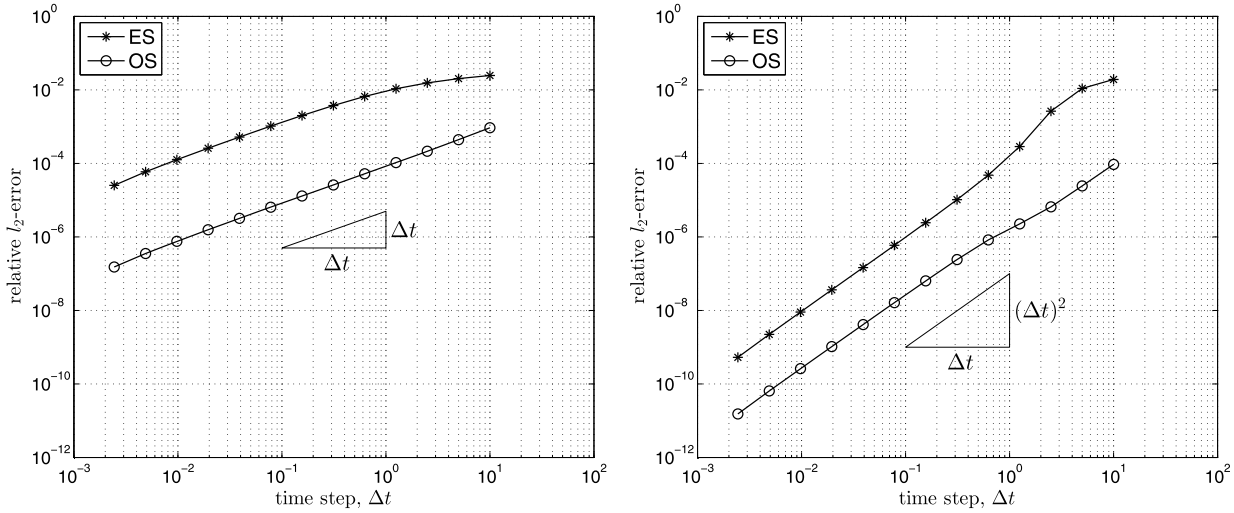

(a) First-order method (b) Second-order method

Fig. 2. Relative l_2-errors at $T_f = 10$ for various time steps with $\epsilon = 0.025$ and $h = 1/3$.

3.2. Analysis of effective time step with a smooth test function in 1D

In [4], Cheng and Warren determined an effective time step Δt_{eff} in the Fourier space and observed that a large time step Δt does not always translate into a significant amount of system evolution in the PFC equation. Similar time scaling effects have been reported also for the Allen–Cahn equation [11,13]. To numerically calculate the effective time step, we take the same initial condition (30) as in the previous section on a domain $\Omega = [0, 32]$. The numerical solution is now computed up to time $T_f = 100$ with $\epsilon = 0.025$ and $h = 1/3$. The tolerance for the iterative step is set to be 10^{-10}. And we take the reference solution with a sufficiently small time step, say $\Delta t = T_f/2^{12}$ in the experiments. Fig. 3 shows the time evolutions of the total energy with $\Delta t = T_f/2^6$, $T_f/2^4$, and $T_f/2^2$. First-order OS and ES methods are used to generate the plots. Using the OS method, the total energy at the same time t are almost the same for different time steps, whereas significant differences emerge with larger time steps for the ES method.

To make the comparison quantitatively, we define the effective time t_{eff} as shown in Fig. 4,

$$\mathcal{E}^{\Delta t}(n\Delta t) = \mathcal{E}^{ref}(t_{eff}),$$

where $\mathcal{E}^{\Delta t}$ is the total energy of the computed solution with a time step Δt and we take the reference total energy $\mathcal{E}^{ref}$ from the reference solution.

Fig. 5(a) shows the time dilation ratios $R(t) = t_{eff}/t$ using different time steps $\Delta t = T_f/2^{10}, T_f/2^8, \ldots, T_f/2^2$ for the first-order ES and OS methods, respectively. For the first-order ES method, the difference between effective t_{eff} and numerical t times becomes bigger and bigger as the time step increases. In this case, the ratio at $t = T_f$ is $R(T_f) \approx 1 - 2 \cdot 10^{-2}\Delta t$ (see Fig. 5(b)). On the other hand, for the first-order OS method, the effective time t_{eff} is almost same as the numerical time

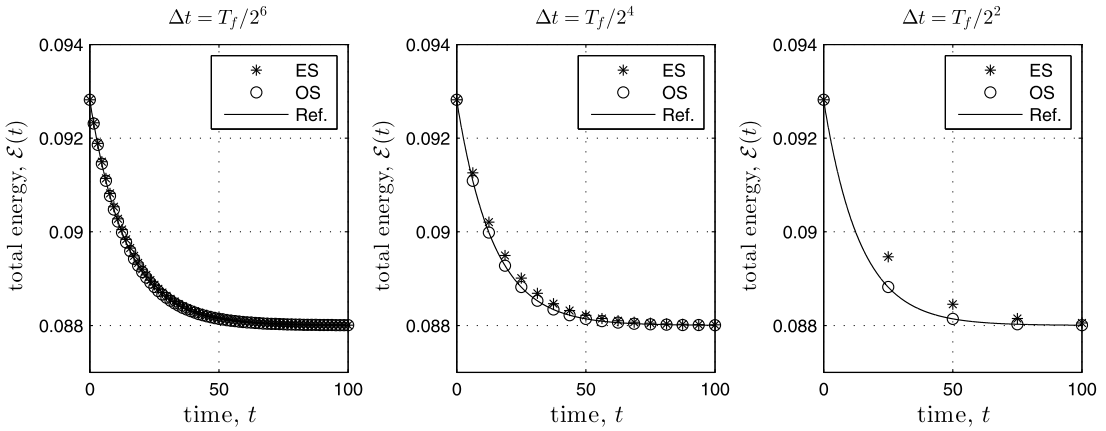

Fig. 3. Time evolutions of the total energy with different time steps. First-order OS and ES methods are used to generate the plots.

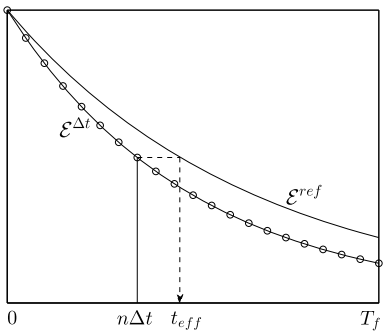

Fig. 4. Definition of the effective time t_{eff}: $\mathcal{E}^{\Delta t}(n\Delta t) = \mathcal{E}^{ref}(t_{eff})$.

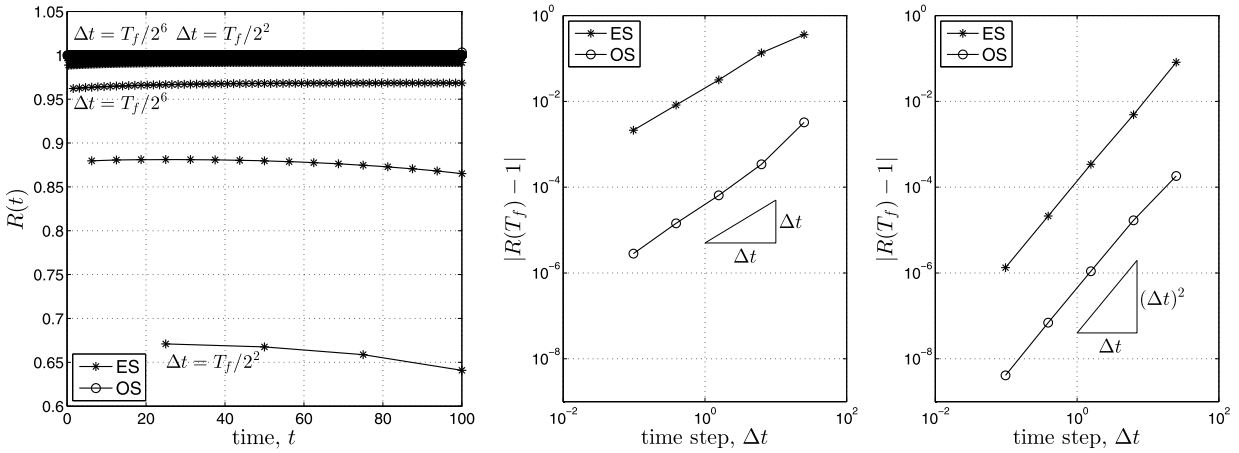

Fig. 5. Time dilation ratio $R(t) = t_{eff}/t$ for $0 \le t \le T_f$=100 using different time steps $\Delta t = T_f/2^{10}, T_f/2^8, \ldots, T_f/2^2$. (a) $R(t)$ for the first-order, (b) $|R(T_f) - 1|$ for the first-order, (c) $|R(T_f) - 1|$ for the second-order method.

t regardless of time step size and the ratio is $R(T_f) \approx 1 + 4 \cdot 10^{-5}\Delta t$. For the second-order ES method, we observe that the ratio decreases to $R(T_f) \approx 1 - 1.5 \cdot 10^{-4}(\Delta t)^2$ (see Fig. 5(c)), but it is still larger than that obtained by the first-order OS method. For the second-order OS method, the ratio is $R(T_f) \approx 1 + 4 \cdot 10^{-7}(\Delta t)^2$.

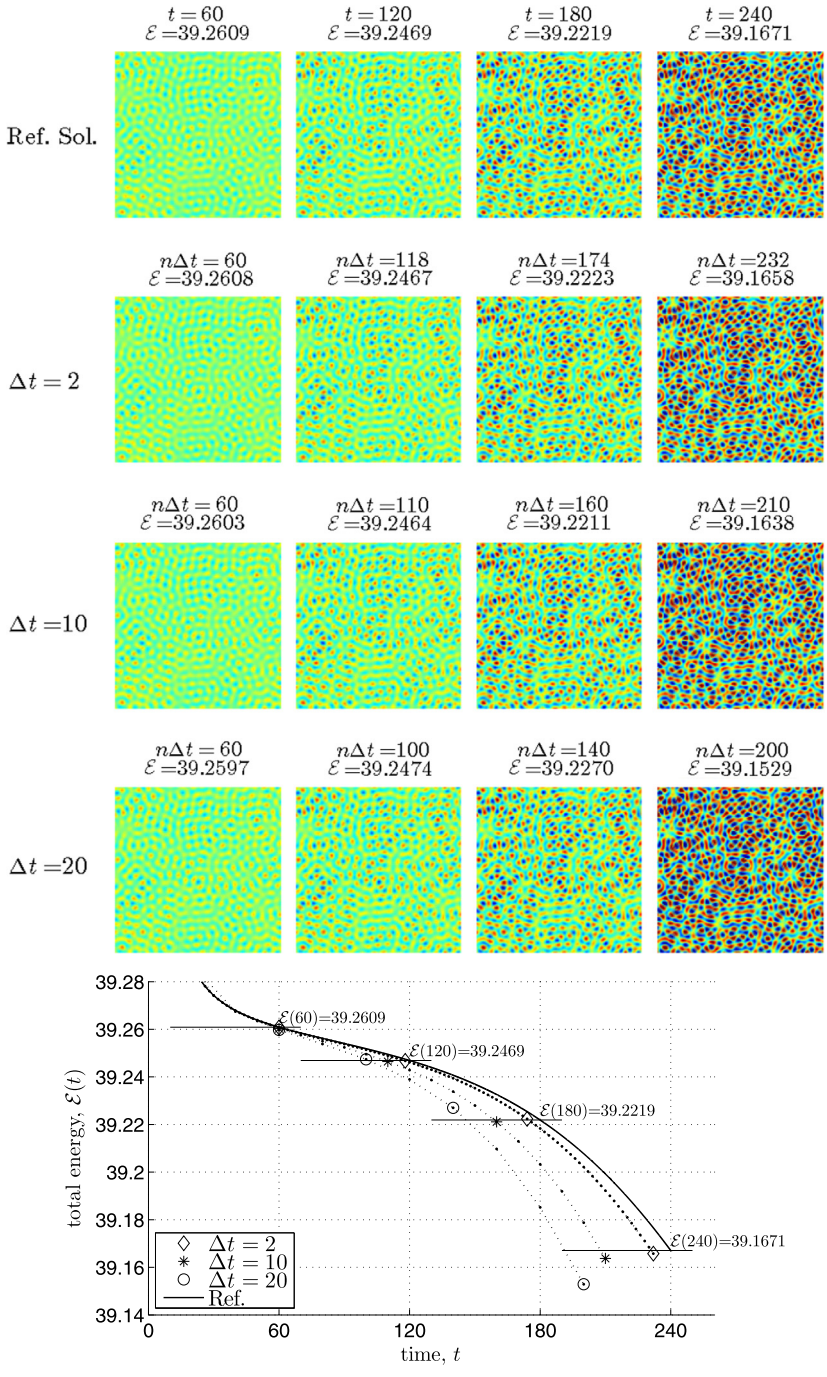

Fig. 6. Total energy $\mathcal{E}(t)$ of the reference solution and total energy $\mathcal{E}(n\Delta t)$ computed by the first-order OS method marked with $(\cdot)$. Four computational results closest to the reference energy $\mathcal{E}(t)$ at $t = 60, 120, 180, 240$ are labeled with markers $(\diamond, *, \circ)$ and the corresponding density fields $\phi(n\Delta t)$ have been shown above. (For interpretation of the references to color in this figure, the reader is referred to the web version of this article.)

3.3. Time evolution of random perturbation in 2D

We now perform a 2D simulation of the PFC equation with $\epsilon = 0.025$ and space grid size $h = 1$ on a domain $\Omega = [0, 128] \times [0, 128]$. The initial condition is set to

$$\phi(x, y, 0) = 0.07 + 0.07 \cdot \text{rand}(x, y),$$

where $\text{rand}(x, y)$ is a randomly chosen number between -1 and 1 but fixed throughout all of the experiments in this subsection. The tolerance for the m-iterative steps is set to be $tol = 10^{-8}$. The simulations are performed by the OS methods

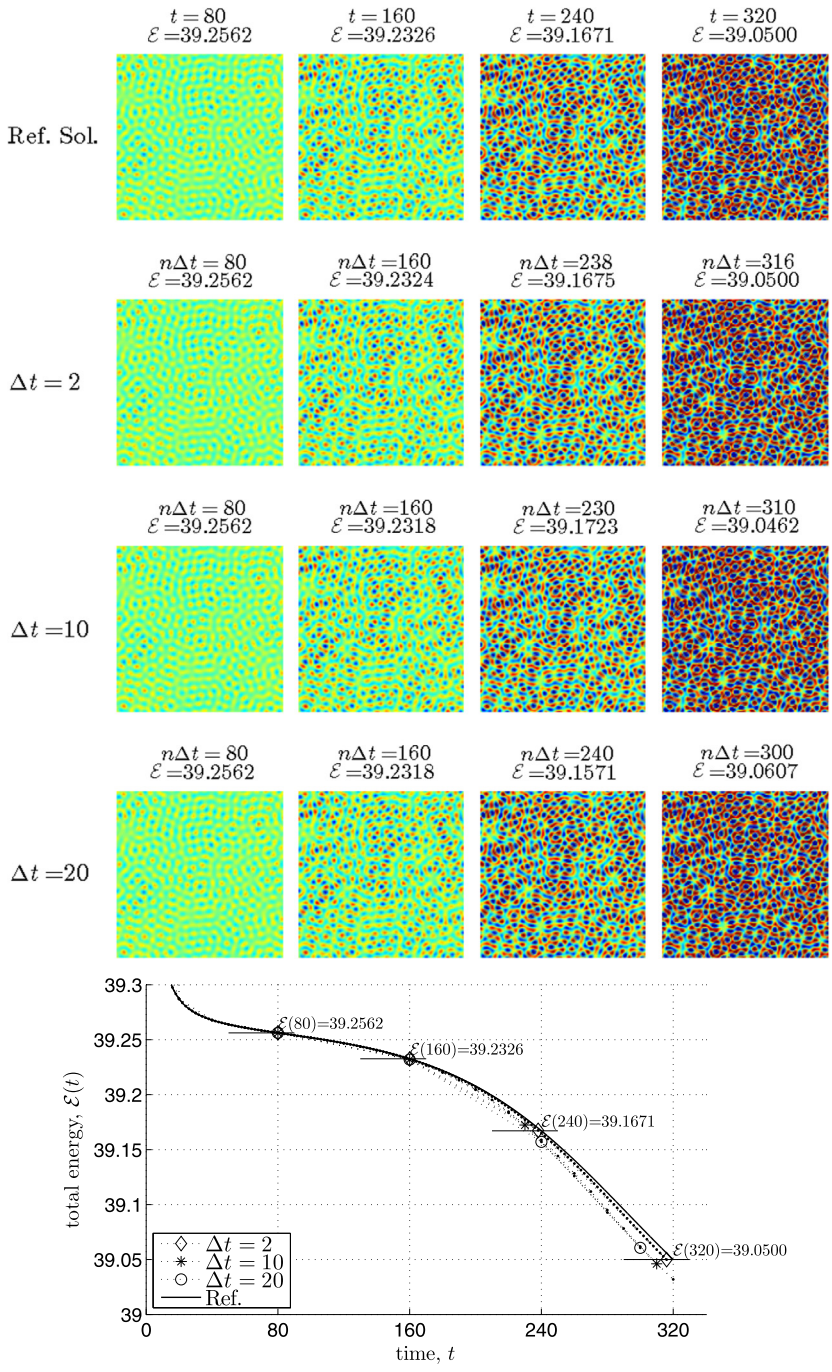

Fig. 7. Total energy $\mathcal{E}(t)$ of the reference solution and total energy $\mathcal{E}(n\Delta t)$ computed by the second-order OS method marked with $(\cdot)$. Four computational results closest to the reference energy $\mathcal{E}(t)$ at $t = 80, 160, 240, 320$ are labeled with markers $(\diamond, *, \circ)$ and the corresponding density fields $\phi(n\Delta t)$ have been shown above. (For interpretation of the references to color in this figure, the reader is referred to the web version of this article.)

with different time steps $\Delta t = 0.01, 2, 10$, and 20 and we consider the numerical solution with $\Delta t = 0.01$ as the reference solution. Figs. 6 and 7 show the time evolutions of the density field ϕ computed by the first- and second-order methods, respectively. In the figure, each rows show the computational results with fixed Δt and snapshots in each column are chosen to match the total energy of the first row (reference solution) as closely as possible. In each snapshots, the red, green, and blue regions indicate $\phi = 0.14$, 0.07, and 0, respectively, and the numerical time and total energy are shown on the top of the subplots.

In [6], the authors observed that the numerical times required to reach the same energy levels using different time steps are dramatically different for the first-order ES method. The times for the second-order ES method are matched much

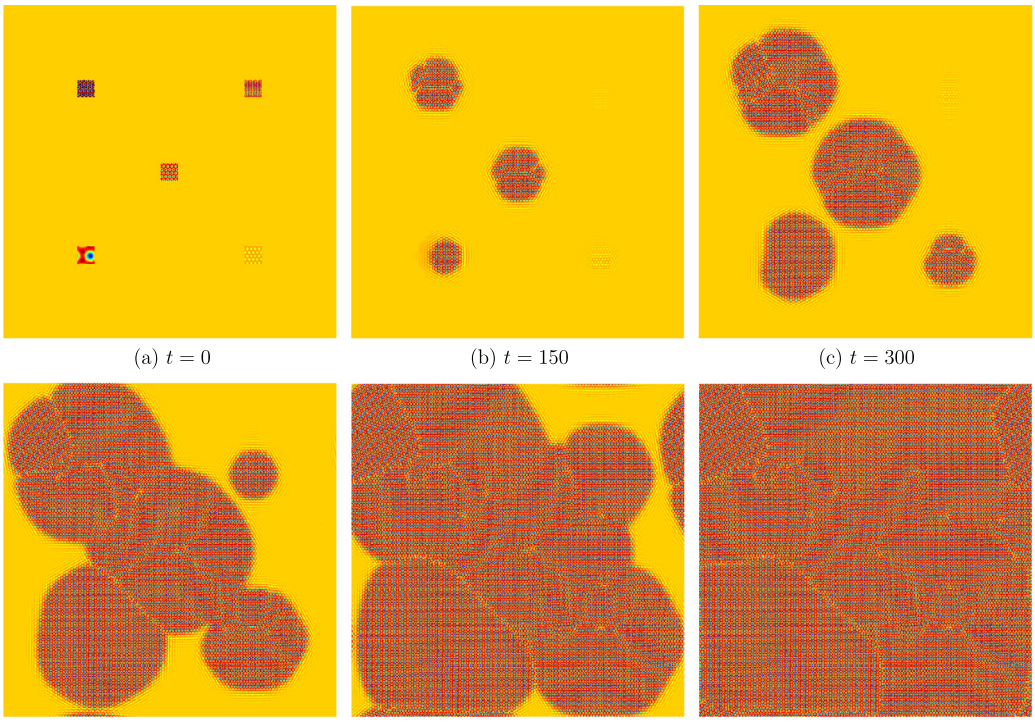

(a) $t = 0$ (b) $t = 150$ (c) $t = 300$

(d) $t = 450$ (e) $t = 600$ (f) $t = 900$

Fig. 8. Heterogeneous nucleation of five crystallites in a supercooled liquid. The snapshots show the density field ϕ at different times. The parameters are $\bar{\phi} = 0.285$, $\epsilon = 0.25$, $\Delta t = 1$, and $h = 1$. The second-order OS method is used in the calculation. (For interpretation of the references to color in this figure, the reader is referred to the web version of this article.)

better than the first-order computation, but a significant difference still exists. From Figs. 6 and 7, we can see that the density fields obtained at the closest energy levels using different time steps are qualitatively similar for both first- and second-order OS methods, and, in particular, the numerical times required to reach the closest energy levels using different time steps are nearly matched for the second-order OS method.

3.4. Crystal growth in a supercooled liquid in 2D

We now use the second-order OS method to simulate the growth of a polycrystal in a supercooled liquid with $\epsilon = 0.25$ on the computational domain $\Omega = [0, 800] \times [0, 800]$. The initial configuration of ϕ shown in Fig. 8(a) consists of five small square patches in a homogeneous environment $\bar{\phi} = 0.285$. We use the following expression to define the density field ϕ in the patch with amplitude A and frequency mode q,

$$\phi(x_l, y_l) = \bar{\phi} + A\left[\cos(qy_l)\cos(\sqrt{3}qx_l) - 0.5\cos(2qy_l)\right],$$

where x_l and y_l define a local system of Cartesian coordinates. We choose the parameters for five patches as $(A, q) = (0.45, q_0)$, $(0.45, 0.25q_0)$, $(0.45, 4q_0)$, $(0.9, q_0)$, $(0.1, q_0)$ where $q_0 = 0.1213\pi$. The lower left and the upper right patch represent lower and higher frequency anomalies, respectively, compared to the center patch. The upper left and the lower right patch have the same frequency mode but the amplitudes are bigger and smaller, respectively.

For the numerical experiment, we also set $\Delta t = 1$ and $h = 1$ and the tolerance for the m-iteration is set to be $tol = 10^{-8}$. Figs. 8(b)–(f) show the snapshots of the density field ϕ at different times. In each figure, the red, green, and blue regions indicate $\phi = 0.6715$, 0, and -0.4746, respectively. The initial configuration evolves into five crystallites, each with a different orientation and a well-defined liquid/crystal interface. As we can see in the figures, the speed of the moving interfaces strongly depends on the patch frequency and amplitude. The frequency and amplitude of the center patch seems to be optimal in the sense that the moving speed of the patch is highest while the higher frequency patch moves with the slowest speed. As time evolves the crystallites impinge upon one another and form grain boundaries.

4. Conclusions

In this paper, we presented the first- and second-order operator splitting (OS) methods for solving the PFC equation. A core idea of the methods was to decompose the original equation into linear and nonlinear subequations, in which the

linear subequation has a closed-form solution in the Fourier space. We applied a nonlinear Newton-type iterative method to solve the nonlinear subequation at the implicit time level. As a result, only 2–3 iterations were involved in proceeding to the next time level. To numerically demonstrate the accuracy and efficiency of the proposed OS methods, we compared with the well-known energy stable (ES) methods. And we observed that the OS methods are more accurate than the ES methods. We also demonstrated the feasibility of the OS methods for the simulation of physical phenomena such as crystal growth.

Acknowledgement

This research was supported by the Basic Science Research Program through the National Research Foundation of Korea (NRF) funded by the Ministry of Education (2009-0093827, 2012-002298).

References

[1] K.R. Elder, M. Katakowski, M. Haataja, M. Grant, Modeling elasticity in crystal growth, Phys. Rev. Lett. 88 (2002) 245701.
[2] K.R. Elder, M. Grant, Modeling elastic and plastic deformations in nonequilibrium processing using phase field crystals, Phys. Rev. E 70 (2004) 051605.
[3] J. Swift, P.C. Hohenberg, Hydrodynamic fluctuations at the convective instability, Phys. Rev. A 15 (1977) 319.
[4] M. Cheng, J.A. Warren, An efficient algorithm for solving the phase field crystal model, J. Comput. Phys. 227 (2008) 6241–6248.
[5] R. Backofen, A. Rätz, A. Voigt, Nucleation and growth by a phase field crystal (PFC) model, Philos. Mag. Lett. 87 (2007) 813–820.
[6] Z. Hu, S.M. Wise, C. Wang, J.S. Lowengrub, Stable and efficient finite-difference nonlinear-multigrid schemes for the phase field crystal equation, J. Comput. Phys. 228 (2009) 5323–5339.
[7] H. Gomez, X. Nogueira, An unconditionally energy-stable method for the phase field crystal equation, Comput. Methods Appl. Mech. Eng. 249–252 (2012) 52–61.
[8] Z. Zhang, Y. Ma, Z. Qiao, An adaptive time-stepping strategy for solving the phase field crystal model, J. Comput. Phys. 249 (2013) 204–215.
[9] G. Strang, On the construction and comparison of difference schemes, SIAM J. Numer. Anal. 5 (1968) 506–517.
[10] D. Goldman, T.J. Kaper, *N*th-order operator splitting schemes and nonreversible systems, SIAM J. Numer. Anal. 33 (1996) 349–367.
[11] H.G. Lee, J.-Y. Lee, A semi-analytical Fourier spectral method for the Allen–Cahn equation, Comput. Math. Appl. 68 (2014) 174–184.
[12] H.G. Lee, J.-Y. Lee, A second order operator splitting method for Allen–Cahn type equations with nonlinear source terms, Physica A 432 (2015) 24–34.
[13] M. Cheng, A.D. Rutenberg, Maximally fast coarsening algorithms, Phys. Rev. E 72 (2005) 055701(R).